

PAT-CNN: Automatic Segmentation and Quantification of Pericardial Adipose Tissue from T2-Weighted Cardiac Magnetic Resonance Images

Zhuoyu Li¹, Camille Petri^{2,3}, James Howard³, Graham Cole³, and Marta Varela^{3*}

¹ Department of Metabolism, Digestion & Reproduction, Imperial College London, UK

² Department of Computing, Imperial College London, UK

³ National Heart & Lung Institute, Imperial College London, UK
*marta.mvarela@imperial.ac.uk

Abstract. Background: Increased pericardial adipose tissue (PAT) is associated with many types of cardiovascular disease (CVD). Although cardiac magnetic resonance images (CMRI) are often acquired in patients with CVD, there are currently no tools to automatically identify and quantify PAT from CMRI. The aim of this study was to create a neural network to segment PAT from T2-weighted CMRI and explore the correlations between PAT volumes (PATV) and CVD outcomes and mortality.

Methods: We trained and tested a deep learning model, PAT-CNN, to segment PAT on T2-weighted cardiac MR images. Using the segmentations from PAT-CNN, we automatically calculated PATV on images from 391 patients. We analysed correlations between PATV and CVD diagnosis and 1-year mortality post-imaging.

Results: PAT-CNN was able to accurately segment PAT with Dice score/ Hausdorff distances of $0.74 \pm 0.03/27.1 \pm 10.9$ mm, similar to the values obtained when comparing the segmentations of two independent human observers ($0.76 \pm 0.06/21.2 \pm 10.3$ mm). Regression models showed that, independently of sex and body-mass index, PATV is significantly positively correlated with a diagnosis of CVD and with 1-year all cause mortality (p-value <0.01).

Conclusions: PAT-CNN can segment PAT from T2-weighted CMR images automatically and accurately. Increased PATV as measured automatically from CMRI is significantly associated with the presence of CVD and can independently predict 1-year mortality.

Keywords: Cardiac MRI · Segmentation · Pericardial Fat Volume · Cardiovascular Disease Risk Factors · Convolutional Neural Network

1 Introduction

Large volumes of pericardial adipose tissue, PAT, and endocardial adipose tissue, EAT, predispose to a number of cardiovascular conditions [24] such as atrial fib-

rillation [8]. This is due to the high metabolic activity of adipose tissue which can stimulate remodelling in cardiac muscle, leading to fibrosis, chamber enlargement and inflammation, among others. PAT can also regulate cardiac tissue innervation [16] likely pro-arrhythmically. Obese patients usually have large amounts of PAT, but correlations between cardiac fat volume and body mass index (BMI) are relatively weak [8, 10].

So far, PAT has been predominantly segmented and quantified using computed tomography (CT) [1]. In these images, fat’s low Hounsfield number allows for comparatively straightforward identification and segmentation using simple intensity threshold-based methods such as region growing and active contours [22] or more complicated approaches like neural networks [5]. Fat is in general more difficult to segment in Cardiac Magnetic Resonance Images (CMRI), where its intensity is much more variable and similar to other tissues’. Quantification of PAT volume (PATV) from MRI has so far only been reported using time-consuming manual segmentation of PAT [6] or dedicated CMRI sequences [7] such as Dixon imaging [10, 12]. This prevents widespread quantification of PATV from more common types of CMRI, despite CMRI’s increasing prominence in the diagnosis and assessment of cardiovascular disease (CVD). A tool to rapidly and accurately quantify PAT from CMRI would allow rapid quantification of PATV in the clinic, to aid CVD risk assessment.

MRI segmentation Convolutional neural networks (CNNs) have shown great ability to segment MR images, enabling easy quantification of several imaging biomarkers whose analysis would otherwise be too time consuming. They consistently outperform non-learned techniques such as thresholding [20], region growing [19] and probability graph models [9]. Once trained, CNNs can perform image analysis in real time in the clinic. To date, and to the best of our knowledge, there are no CNN-based tools for the segmentation of PAT from T2-weighted CMR images.

Aims In this project, we aim to estimate PATV from clinical CMRI. We focus on axial T2-weighted rapid gradient-echo scans which are routinely acquired in the clinic and in which CNNs have been used to accurately segment several cardiac structures [11]. We initially create a non-learned semi-automatic image processing protocol to segment PAT and generate training data for the proposed CNN. We then train and test a dedicated CNN to segment PAT in these images. Finally, using data from 391 patients, we investigate correlations between: a) PATV and the presence of CVD and b) PATV and 1-year all-cause mortality.

2 Methods

Data We uses fully anonymized T2-prepared spoiled GRE axial stacks acquired at 1.5T (TE: 1.56 ms, TR: 3.1 ms, recon voxel size: $1.4 \times 1.4 \times 6.0 \text{ mm}^3$) in 391 patients with known or suspected CVD, under ethical approval. The number of slices in each volumetric scan ranged from 23 to 55.

Preprocessing Ground truth PAT segmentation was semi-automatically performed in 70 training images (Fig 1). As the first step, we identified the

cardiac chambers and left ventricular (LV) myocardium using HRNet, an existing CNN trained in T2-weighted images with a similar contrast [11]. Using these segmentations, we created a bounding box around the heart. We then performed a 2-class Otsu segmentation [21] on the cropped images. In most cases, one of the classes roughly coincided with subcutaneous fat, allowing the rapid segmentation of PAT after some further manual corrections. These semi-automatic PAT segmentations were reviewed by a second independent observer.

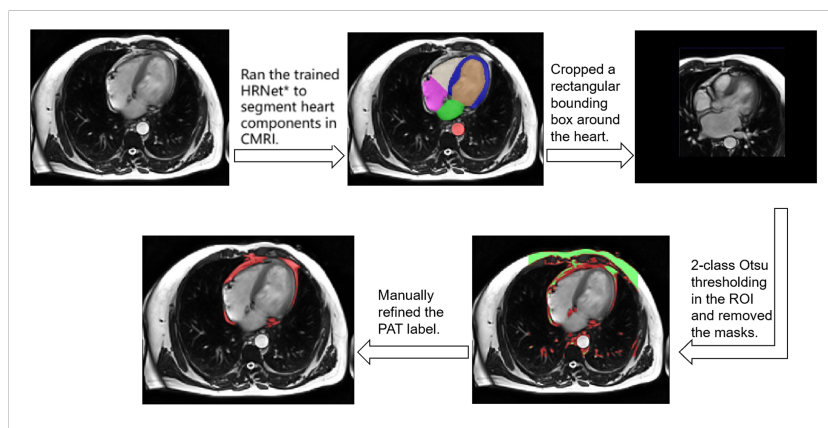


Fig. 1. Semi-automatic pipeline for ground truth PAT segmentation. ROI: Region of Interest

Model: Architecture To allow fully automatic PAT labelling, we trained PAT-CNN, a 3D Res-UNet CNN [13]. The network (shown in Fig 2) included a contracting path with four convolutional layers, an expanding path with four upsampling layers and concatenate connections. A residual unit was added to each layer. In residual units, batch normalization and parametric rectified linear unit (PReLU) were implemented to improve the feature selection results. The output layer used a sigmoid function as the activation function and was trained to classify each pixel as: PAT (label 1) or background/other tissues (label 0).

Model: Dataset Setup 70 scans with manual PAT labels were randomly divided into a training+validation dataset (60 images) and a testing dataset (10 images). A second independent observer independently segmented PAT in the test dataset to assess inter-observer segmentation metrics.

Model: Data Augmentation To enhance PAT-CNN’s invariance and generalization, as well as expand the size of the dataset, we applied data augmentation during training using the image analysis library SimpleITK [25]. We randomly applied rotation, crop, flip, blur and Rayleigh noise addition to each input image of the network in each epoch. The probability of each transformation was 0.1.

Model: Loss Function The loss function combined cross-entropy loss and Dice loss terms [26]. The Dice loss term help improves PAT-CNN’s accuracy

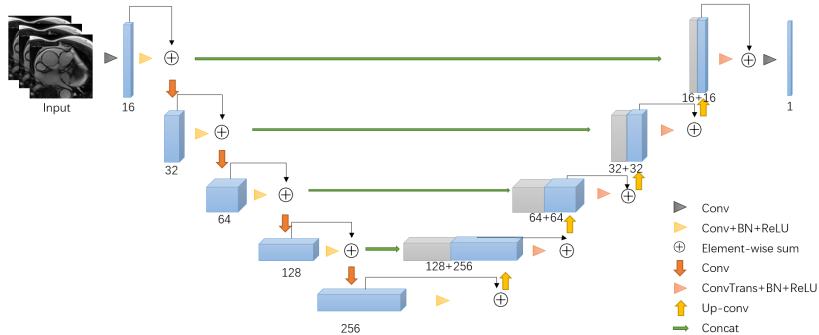


Fig. 2. Structure diagram of PAT-CNN. The kernel sizes of convolutions and transpose convolutions are $3 \times 3 \times 3$. The numbers represent filters numbers in each layer. The triangle arrows represents the residual units.

in the presence of the large imbalance between the volumes of PAT and voxels labelled as background/other organs. The cross-entropy loss term minimises the likely instability of the gradients of a pure Dice-score-based loss function. The total loss function can be represented as below, where x_n is the ground truth label of the n^{th} sample, y_n is its prediction, N is the total number of samples (and the small term ϵ in the Dice coefficient is used to avoid the denominator becoming 0):

$$Loss(X, Y) = 1 - \frac{2 \sum_{n=1}^N x_n y_n + \epsilon}{\sum_{n=1}^N x_n + \sum_{n=1}^N y_n + \epsilon} - \frac{1}{N} \sum_{n=1}^N x_n \log(y_n) \quad (1)$$

Model: Hyperparameters and Performance Assessment Through our experimental results, the optimal batch size was 8. We used Adam [15] and set the learning rate to 10^{-4} , training for 60 epochs. This combination performed best on the validation dataset. We used the Dice Score and Hausdorff Distance to evaluate PAT-CNNs performance on the test dataset. Using these metrics, we additionally compared PAT-CNN to the vanilla U-Net [23] commonly using for segmenting medical images.

Statistical Analysis: Data We used PAT-CNN to estimate PATV (in cm^3) in all 391 volumetric T2-weighted axial CMR images. From the anonymized imaging metadata and radiology reports, we extracted the following demographic information (*mean* \pm *std*): age (55 ± 18 years), sex (42% female), BMI (27.7 ± 5.9 kg/m^2) and 1-year post-scan mortality (‘Deceased’, 8.2%). We also compiled diagnostic information, which was synthesised into 73 binary clinical diagnostic labels (presence/absence of: dilated cardiomyopathy, left/right ventricular failure, left/right ventricular hypertrophy, myocardial infarction, ischaemia, etc). The sum of these diagnostic labels was compiled into a single variable ‘CVD Diagnosis’ (2.9 ± 1.9).

Statistical Analysis: Methods We investigated the relationship between the regressor variables: PATV, sex, age and BMI and the dependent variables:

‘CVD diagnosis’, ‘Deceased’ and PATV, using univariate Pearson/phi correlation analysis. Those regressors that were significantly correlated ($\alpha = 0.01$) with the independent variables were then used as inputs to a multivariate analysis using ordinary least squares (for the ‘CVD Diagnosis’ and ‘PATV’ dependent variables) and a logistic regression model (for the dichotomous variable ‘Deceased’). We note that the clinical dataset used did not include time-to-mortality information and survival analyses were therefore not performed.

3 Results

PAT-CNN Performance On the test dataset, PAT was segmented with an average Dice score/Hausdorff distance of $0.74 \pm 0.03/27.1 \pm 10.9$ mm. The model coped well with variations in PAT shape, size and location (Fig 3) and the presence of pathological changes. PAT-CNN performed better than U-Net and its results compared well with the agreement between two human operators on the same dataset (Table 1).

	PAT-CNN	U-Net	Observer 2
Dice Score	0.74 ± 0.03	0.71 ± 0.03	0.76 ± 0.06
Hausdorff Distance (mm)	27.1 ± 10.9	32.8 ± 11.2	21.2 ± 10.3

Table 1. Performance of PAT-CNN, U-Net and a second human observer on the test images. (The segmentations from human Observer 1 were treated as the ground truth for this analysis.)

Statistical Analysis Across the 391 analysed patients, PATV had a mean of 139.60 cm^3 and a standard deviation of 80.24 cm^3 , in excellent agreement with PAT quantification from CT [5]. PATV is significantly correlated with patients’ age ($\rho_{Pearson} = 0.38$), sex and BMI ($\rho_{Pearson} = 0.34$), but in a multivariate analysis, only sex and BMI remain significant (Table 2). PATV and age were the only regressor variables found to be significantly correlated to both CVD diagnostic labels and 1-year mortality post-imaging in both univariate and multivariate analyses (Table 2). This is in contrast to BMI which was not an independent predictor of either mortality or CVD diagnosis in univariate analysis (Table 2).

4 Discussion

We present PAT-CNN, a CNN able to identify PAT accurately in T2-weighted CMRI across subjects of various sizes and in the presence of different types of pathology. PATV estimated using PAT-CNN’s segmentation of CMRI is significantly correlated to the presence of cardiac pathology and is an independent predictor of 1-year mortality, as seen in studies from the literature in which PAT was segmented manually [8].

	PATV (cm^3)	Deceased	CVD Diagnosis
Sex	-50.2*		-0.30
Age (years)	1.70	0.03*	0.02*
BMI (kg/m^2)	3.92*		
PATV (cm^3)		0.01*	0.01*

Table 2. Regression coefficients from 3 multivariate regression analyses ($n = 391$), for the dependent variables listed in each column.

Each row shows each regressor considered in the model. (For the dichotomous variable ‘Sex’, females are represented by 1 and males by 0.) Only regressors found to be statistically significant in univariate analyses were considered. Entries are the regression coefficients in the specified units, with the asterix (*) denoting significant correlations at $\alpha = 0.01$. PATV: pericardial adipose tissue volume; BMI: body-mass index; CVD: cardiovascular disease.

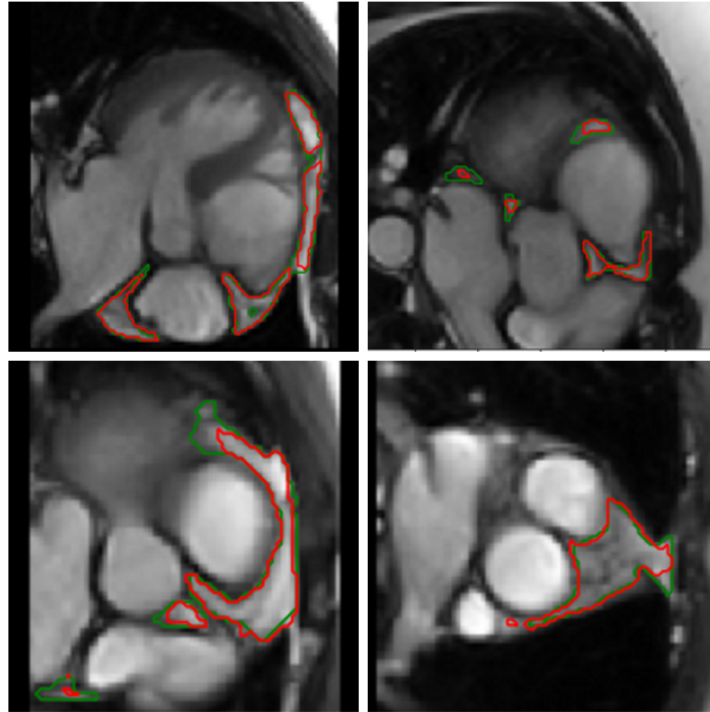


Fig. 3. Representative examples of T2-weighted slices from four different patients overlaid with the contours for the ground truth (red) and PAT-CNN (green) PAT labels.

PAT Segmentation PAT is distributed around in the heart in several non-contiguous patches with various shapes, making PAT segmentation more complex than the segmentation of contiguous and less variable structures such as the cardiac chambers themselves. Moreover, when present, pericardial fluid can

easily be mistakenly labelled as PAT, as fluid and fat have a similar intensity and appearance on T2-weighted CMR images.

Despite the difficulty of the task, PAT-CNN was able to segment PAT with an average Dice score of 0.74, outperforming U-Net and performing only marginally worse than the average Dice score of 0.76 obtained when comparing the segmentations from different human observers (see Table 1).

PAT-CNN uses a 3D Res-UNet previously used to segment heart chambers [14, 18], with a modified combined Dice-Cross-Entropy loss that outperformed Dice-only and Cross-Entropy-only losses for this task. We therefore show that the 3D Res-UNet has a good performance in CMRI even when segmenting irregular, non-connected regions such as PAT.

Statistical Analysis of PATV

PATV estimated automatically using PAT-CNN shows similar correlations to clinical variables as PATV estimated from CT and echocardiography [2, 17]. Females, elderly people and those with higher BMI are more likely to have more PATV. Statistically significant correlations were found between PATV and a diagnosis of cardiovascular disease at the time of scan, as has been reported in other studies [2]. PATV was also an independent predictor of one-year all-cause mortality in the analysed 319 subjects, as also found on CT [4]. Interestingly, BMI was not a predictor for mortality or the presence of CVD, although it was significantly but weakly correlated with PAT ($\rho_{Pearson} = 0.34$), also as seen in other studies [2, 10].

Our analysis used 1-year all-cause mortality, as we could not obtain information about CVD-related deaths or temporal information about the time to death. Body surface area (BSA) is more commonly used than BMI for the indexing of cardiac function variables. BSA would have been an interesting variable to include in our regression models, but it was not available in our dataset.

Future Work PAT segmentations, such as those provided by PAT-CNN, provide information beyond that of PATV alone. In the current study, we did not analyse the clinical importance of the location or spatial distribution of PAT, which is likely to have clinical value beyond PAT volume only. We also did not attempt to index PATV by body area or heart size, which may yield biomarkers with further clinical value [3].

Alongside PAT, epicardial adipose tissue (EAT) is also likely to play an important role in cardiovascular pathophysiology and it should be identifiable in CMRI. EAT, however, is expected to deposit in regions of smaller volume and its identification is limited by partial volume effects at MRI’s typical spatial resolution. EAT’s reliable identification would require MRI at much higher spatial resolution or the use of specialised CMRI sequences such as Dixon techniques [10, 12]. Dixon technique CMR images are not usually acquired as part of clinical examinations, stressing the importance of our approach to automatically segment PAT from commonly acquired T2-weighted clinical scans.

Pending training and testing across images from different sites and scanners, PAT-CNN can be deployed as a scanner-side analysis tool to automatically estimate PATV. It can also be used to explore the mechanisms of different CVDs

by highlighting potential relationships between PAT volume and location and CVD manifestations.

5 Conclusions

We propose PAT-CNN, a neural network to automatically segment PAT from CMR images. We show that PAT segmentations are reliable, making PAT-CNN ready to be deployed on clinical images to yield biomarkers of potential clinical interest. Using data from 391 patients, we find that PAT volume, estimated using PAT-CNN, is significantly correlated with both a diagnosis of CVD and 1-year all-cause mortality, independently of sex and BMI.

Acknowledgements

This work was supported by the British Heart Foundation Centre of Research Excellence at Imperial College London (RE/18/4/34215).

References

1. Benčević, M., Galić, I., Habijan, M., Pižurica, A.: Recent Progress in Epicardial and Pericardial Adipose Tissue Segmentation and Quantification Based on Deep Learning: A Systematic Review. *Applied Sciences* **12**(10), 5217 (2022). <https://doi.org/10.3390/app12105217>
2. Britton, K.A., Massaro, J.M., Murabito, J.M., Kreger, B.E., Hoffmann, U., Fox, C.S.: Body Fat Distribution, Incident Cardiovascular Disease, Cancer, and All-Cause Mortality. *Journal of the American College of Cardiology* **62**(10), 921–925 (9 2013). <https://doi.org/10.1016/J.JACC.2013.06.027>
3. Cai, S., Wald, R., Deva, D.P., Kiaii, M., Ng, M.Y., Karur, G.R., Bello, O., Li, Z.J., Leipsic, J., Jimenez-Juan, L., Kirpalani, A., Connelly, K.A., Yan, A.T.: Cardiac MRI measurements of pericardial adipose tissue volumes in patients on in-centre nocturnal hemodialysis. *Journal of Nephrology* **33**(2), 355–363 (4 2020). <https://doi.org/10.1007/s40620-019-00665-4>
4. Cheng, V.Y., Dey, D., Tamarappoo, B., Nakazato, R., Gransar, H., Miranda-Peats, R., Ramesh, A., Wong, N.D., Shaw, L.J., Slomka, P.J., Berman, D.S.: Pericardial Fat Burden on ECG-Gated Noncontrast CT in Asymptomatic Patients Who Subsequently Experience Adverse Cardiovascular Events. *JACC: Cardiovascular Imaging* **3**(4), 352–360 (4 2010). <https://doi.org/10.1016/J.JCMG.2009.12.013>
5. Commandeur, F., Goeller, M., Betancur, J., Cadet, S., Doris, M., Chen, X., Berman, D.S., Slomka, P.J., Tamarappoo, B.K., Dey, D.: Deep Learning for Quantification of Epicardial and Thoracic Adipose Tissue from Non-Contrast CT. *IEEE Transactions on Medical Imaging* **37**(8), 1835–1846 (8 2018). <https://doi.org/10.1109/TMI.2018.2804799>
6. Davidovich, D., Gastaldelli, A., Sicari, R.: Imaging cardiac fat. *European Heart Journal - Cardiovascular Imaging* **14**(7), 625–630 (7 2013). <https://doi.org/10.1093/EHJCI/JET045>

7. Ding, X., Pang, J., Ren, Z., Diaz-Zamudio, M., Jiang, C., Fan, Z., Berman, D.S., Li, D., Terzopoulos, D., Slomka, P.J., Dey, D.: Automated pericardial fat quantification from coronary magnetic resonance angiography: feasibility study. *Journal of Medical Imaging* **3**(1), 014002 (2016). <https://doi.org/10.1117/1.jmi.3.1.014002>, <https://doi.org/10.1117/1.jmi.3.1.014002>
8. Fitzgibbons, T.P., Czech, M.P.: Epicardial and Perivascular Adipose Tissues and Their Influence on Cardiovascular Disease: Basic Mechanisms and Clinical Associations. *Journal of the American Heart Association* **3**(2) (3 2014). <https://doi.org/10.1161/JAHA.113.000582>
9. Grosgeorge, D., Petitjean, C., Dacher, J.N., Ruan, S.: Graph cut segmentation with a statistical shape model in cardiac MRI. *Computer Vision and Image Understanding* **117**(9), 1027–1035 (2013). <https://doi.org/https://doi.org/10.1016/j.cviu.2013.01.014>
10. Henningsson, M., Brundin, M., Scheffel, T., Edin, C., Viola, F., Carlhäll, C.J.: Quantification of epicardial fat using 3D cine Dixon MRI. *BMC Medical Imaging* **20**(1), 1–9 (7 2020). <https://doi.org/10.1186/s12880-020-00478-z>
11. Howard, J., Zaman, S., Ragavan, A., Hall, K., Leonard, G., Sutanto, S., Ramadoss, V., Razvi, Y., Linton, N.F., Bharath, A., Shun-Shin, M.J., Rueckert, D., Francis, D., Cole, G.: Automated analysis and detection of abnormalities in transaxial anatomical cardiovascular magnetic resonance images: a proof of concept study with potential to optimize image acquisition. *International Journal of Cardiovascular Imaging* **37**(3), 1033–1042 (2021). <https://doi.org/10.1007/s10554-020-02050-w>
12. Kellman, P., Hernando, D., Shah, S., Zuehlsdorff, S., Jerecic, R., Mancini, C., Liang, Z.P., Arai, A.E.: Multiecho dixon fat and water separation method for detecting fibrofatty infiltration in the myocardium. *Magnetic Resonance in Medicine* **61**(1), 215–221 (1 2009). <https://doi.org/10.1002/mrm.21657>
13. Kerfoot, E., Clough, J., Oksuz, I., Lee, J., King, A.P., Schnabel, J.A.: Left-Ventricle Quantification Using Residual U-Net. *Lecture Notes in Computer Science (including subseries Lecture Notes in Artificial Intelligence and Lecture Notes in Bioinformatics)* **11395 LNCS**, 371–380 (2019). https://doi.org/10.1007/978-3-030-12029-0_40
14. Kerfoot, E., Puyol Anton, E., Ruijsink, B., Clough, J., King, A.P., Schnabel, J.A.: Automated CNN-based reconstruction of short-axis cardiac MR sequence from real-time image data. In: *Lecture Notes in Computer Science (including subseries Lecture Notes in Artificial Intelligence and Lecture Notes in Bioinformatics)*, vol. 11040 LNCS, pp. 32–41. Springer Verlag (2018). https://doi.org/10.1007/978-3-030-00946-5_4
15. Kingma, D., Ba, J.: Adam: A Method for Stochastic Optimization. *Computer Science* (2014)
16. Lavie, C.J., Pandey, A., Lau, D.H., Alpert, M.A., Sanders, P.: THE PRESENT AND FUTURE Obesity and Atrial Fibrillation Prevalence, Pathogenesis, and Prognosis Effects of Weight Loss and Exercise. Tech. rep. (10 2017). <https://doi.org/10.1016/J.JACC.2017.09.002>
17. Liu, J., Fox, C.S., Hickson, D.M., Sarpong, D., Ekunwe, L., May, W.D., Hundley, G.W., Carr, J.J., Taylor, H.A.: Pericardial Adipose Tissue, Atherosclerosis, and Cardiovascular Disease Risk FactorsThe Jackson Heart Study. *Diabetes Care* **33**(7), 1635–1639 (7 2010). <https://doi.org/10.2337/DC10-0245>
18. Lourenço, A., Kerfoot, E., Dibblin, C., Alskaf, E., Anjari, M., Bharath, A.A., King, A.P., Chubb, H., Correia, T.M., Varela, M.: Left Atrial Ejection Fraction Estimation Using SEGANet for Fully Automated Segmentation of CINE

- MRI. In: Lecture Notes in Computer Science (including subseries Lecture Notes in Artificial Intelligence and Lecture Notes in Bioinformatics). vol. 12592 LNCS, pp. 137–145. Springer Science and Business Media Deutschland GmbH (2021). https://doi.org/10.1007/978-3-030-68107-4_14, https://link.springer.com/chapter/10.1007/978-3-030-68107-4_14
19. Mancas, M., Gosselin, B., Macq, B.: Segmentation using a region-growing thresholding. In: Dougherty, E.R., Astola, J.T., Egiazarian, K.O. (eds.) Image Processing: Algorithms and Systems IV. vol. 5672, pp. 388–398. International Society for Optics and Photonics, SPIE (2005). <https://doi.org/10.1117/12.587995>
 20. Norouzi, A., Rahim, M.S.M., Altameem, A., Saba, T., Rad, A.E., Rehman, A., Uddin, M.: Medical Image Segmentation Methods, Algorithms, and Applications. IETE Technical Review **31**(3), 199–213 (2014). <https://doi.org/10.1080/02564602.2014.906861>
 21. Otsu, N.: A Threshold Selection Method from Gray-Level Histograms. IEEE Transactions on Systems, Man, and Cybernetics **9**(1), 62–66 (1979). <https://doi.org/10.1109/TSMC.1979.4310076>
 22. Rodrigues, O., Morais, F.F., Morais, N.A., Conci, L.S., Neto, L.V., Conci, A.: A novel approach for the automated segmentation and volume quantification of cardiac fats on computed tomography. Computer Methods and Programs in Biomedicine **123**, 109–128 (1 2016). <https://doi.org/10.1016/J.CMPB.2015.09.017>
 23. Ronneberger, O., Fischer, P., Brox, T.: U-Net: Convolutional Networks for Biomedical Image Segmentation. pp. 234–241. Springer, Cham (2015). https://doi.org/10.1007/978-3-319-24574-4_28, http://link.springer.com/10.1007/978-3-319-24574-4_28
 24. Weschenfelder, C., Quadros, A., Santos, J., Garofallo, S.B., Marcadenti, A.: Adipokines and Adipose Tissue-Related Metabolites, Nuts and Cardiovascular Disease. Metabolites **10**(1), 32– (2020)
 25. Yaniv, Z., Lowekamp, B.C., Johnson, H.J., Beare, R.: {SimpleITK} Image-Analysis Notebooks: a Collaborative Environment for Education and Reproducible Research. Journal of Digital Imaging **31**(3), 290–303 (2018). <https://doi.org/10.1007/s10278-017-0037-8>
 26. Yeung, M., Sala, E., Schönlieb, C.B., Rundo, L.: Unified Focal loss: Generalising Dice and cross entropy-based losses to handle class imbalanced medical image segmentation. Computerized Medical Imaging and Graphics **95**, 102026 (1 2022). <https://doi.org/10.1016/J.COMPMEDIMAG.2021.102026>